NUCL SCI TECH (2022) 33:13
https://doi.org/10.1007/s41365-022-00990-7

Modular next generation fast-neutron detector for portal monitoring

E. Aboud[1,2] · S. Ahn[1] · G. V. Rogachev[1,2] · V. E. Johnson[3] · J. Bishop[1,2] · G. Christian[1,2] · E. Koshchiy[1] · C. E. Parker[1] · D. P. Scriven[1,2]

Received: 12 October 2021 / Revised: 4 December 2021 / Accepted: 11 December 2021 / Published online: 29 January 2022

Abstract Nuclear nonproliferation is of critical importance for global security. Dangerous fissile materials including highly enriched uranium and weapons-grade plutonium are especially important to detect. Active interrogation techniques may result in much better sensitivity but are difficult with conventional portal monitors that rely on detecting thermal neutrons. Also, most conventional portal monitoring systems rely on ^{3}He, which has a finite and continually decreasing supply. By designing a highly segmented array of organic scintillators, we posit that we can accurately and quickly identify fissile materials, including weapons-grade plutonium and highly enriched uranium, being smuggled. We propose a new design for a fast-neutron detector that overcomes the limitations of the current generation of portal monitors. MCNP6 simulations have been performed in conjunction with the UMPBT statistical model to determine the sensitivity limitations of the proposed detector. Results suggest that the proposed detector may be ~ 10 times more efficient than current-generation thermal neutron detectors and may be able to positively identify a ~ 81 mg ^{235}U source in as little as 192 seconds utilizing active interrogation techniques.

Keywords Fast-neutron detection · Portal monitoring · Nonproliferation

1 Introduction

Monitoring and halting the movement of unauthorized fissile materials become more important every day, specifically the monitoring of special nuclear materials (SNM). SNMs include ^{239}Pu, which is the primary component of weapons-grade plutonium (WGPu), and ^{235}U, which is the primary component of highly enriched uranium (HEU). These are radioactive materials and can be identified using γ and neutron detectors. Neutron detection is typically used together with γ-ray monitoring and has an advantage of lower natural background and background induced by radioactive materials used in industry and for medical applications. While WGPu emits significant amount of neutrons and is easier to detect, HEU is particularly challenging because of the low neutron emission rate and due to the fact that low energy γ-rays produced by HEU are relatively easy to shield. Portal monitoring systems often combine γ-ray detectors and neutron detectors. Due to naturally occurring radioactive materials and

This material is based upon work was supported by the National Nuclear Security Administration (NNSA) through the Center for Excellence in Nuclear Training and University Based Research (CENTAUR) under Award No. DE-NA0003841, by the U.S.Department of Energy, Office of Science, Office of Nuclear Physics, under Award No. DE-FG02-93ER40773, and the College of Science at Texas A&M University through Strategic Transformative Research Program (CoS STRP). E. Aboud acknowledges funding through the Nuclear Solutions Institute's Graduate Student Merit Fellowship.

✉ E. Aboud
eaboud@physics.tamu.edu

[1] Cyclotron Institute, Texas A&M University, College Station, TX 77843, USA

[2] Department of Physics and Astronomy, Texas A&M University, College Station, TX 77843, USA

[3] Department of Statistics, Texas A&M University, College Station, TX 77843, USA

electronic noise or failures, in radiation portal monitors, the false alarm rate for γ-rays is about 1 in 10^2 and for neutrons about 1 in 10^4 [1].

Current neutron portal monitoring techniques rely heavily on thermal neutron detectors, many of which require ^{3}He. ^{3}He has applications in many different fields, which has dwindled the increasingly small and finite terrestrial supply [2]. Therefore, ^{3}He is becoming increasingly expensive and hard to acquire [3, 4]. Efforts to move away from ^{3}He detectors have been an area of interest for more than a decade now.

Generally, SNMs of interest emit neutrons with average energies around 1 MeV – the fast-neutron region. Thermal neutron detectors rely on moderating fast neutrons to detect them, making them indistinguishable from ambient thermal neutrons. These detectors use total counting techniques, which are not position sensitive, to determine an increase in total neutron flux. Detecting only the total neutron flux does not allow them to be sensitive to low-emission fissile materials [5–7]. These techniques may also be prone to a high false alarm rate.

Active interrogation techniques can be used to enhance the sensitivity to SNMs such as HEU and WGPu. Fission can be induced in these materials by using a low-energy neutron generator, which utilizes reactions such as ^{7}Li(p,n)^{7}Be to produce neutrons. A beam of neutrons with energy around few tens of keV may induce fission in ^{235}U and ^{239}Pu, while not inducing fission in other isotopes such as ^{238}U and ^{232}Th. The 60-keV neutron beam produces a small dose and can penetrate bulk materials nearly as well as higher energy neutrons. These low-energy neutrons also lose their energy primarily from elastic collisions rather than reactions or inelastic scattering, creating an easily identifiable neutron background. Previous studies have shown positive results in the identification of small quantities of ^{235}U, even when shielded by various materials [8–10].

Recently, there have been attempts to combat the limitations of monitoring systems based on thermal neutron detection [11–13]. Hausladen et al. [13] use a segmented array of liquid scintillators with pinhole apertures. PMT after-pulsing caused the liquid scintillator setup to perform worse than expected for neutron and γ-ray pulse shape discrimination. Source identification tested well for high-rate sources, but may have difficulty with lower-rate sources.

The approach of Rose et al. [11] uses high-energy γ-ray ($E_\gamma > 4$ MeV) and fast-neutron active interrogation for spatial imaging. Both the high-energy γ rays and the fast neutrons can induce fission in SNM. However, the high-intensity background inhibits the ability for direct detection and forces the reliance on secondary reactions, including β-decay measurements.

Hamel et al. proposed a dual-particle imager (DPI), which can localize both neutrons and γ rays. A neutron generator can be used to induce fission and generated neutron events may be discarded using a veto. Image reconstruction was done for both neutrons and γ rays using the stochastic origin ensemble statistical technique with the simple backprojection method [14]. Image reconstruction can localize the source, but does not reliably identify the source. After localization, source identification is done by analyzing the intensity decay time, while the neutron generator is off. The DPI method can localize and identify SNM, but it requires a multi-step analysis and can take a significant amount of time to identify the source [12].

In order to resolve the existing limitations, we developed a new direct technique for fast-neutron portal monitoring that overcomes the sensitivity limitations of fast-neutron thermalization and allows for the use of active-interrogation techniques. By using small hydrocarbon (*p*-terphenyl) scintillators in a large array, we are able to detect fast neutrons to localize fissile materials, including HEU and WGPu. Our novel design, combined with Bayesian statistical analysis, can perform with an efficiency that is a factor of 12 better than the standard technique based on ^{3}He-tubes with a moderator, even for passive interrogation. Insensitivity of this detector to low-energy neutrons makes it ideal for applications that involve active interrogation. The results described in this paper are intended as proof of viability calculations. A prototype detector is being built and will become available in the near future. The pulse shape discrimination thresholds and time resolution that are used in the simulations presented below were adopted from the already existing basic units of this detector.

2 Simulated detector design

Our proposed design took inspiration from the Gamma-Ray Burst Monitor [15]. Similar to their design of identifying an astrophysical event, we utilize small modular crystals to localize a radioactive source. Our conceptual device consists of an array of $2.5 \times 2.5 \times 2.5$ cm^3 *p*-terphenyl crystals. The detector size is approximately 50×50 cm^2 in cross section and 25-cm deep — 4000 crystals in total. The cross section size was chosen for prototyping purposes, and the depth was chosen to be approximately two mean free paths of a 1 MeV neutron in *p*-terphenyl (Fig. 1). The scintillators are grouped into layers of one crystal in height (Fig. 2). Each of the layers is

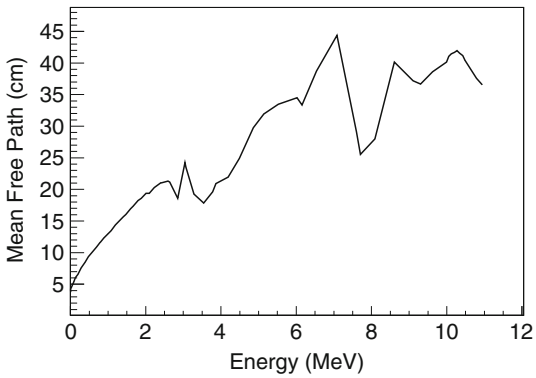

Fig. 1 The mean free path of neutrons through *p*-terphenyl until the first collision for a range of energies up to approximately 11 MeV. The cross section data were taken from ENDF libraries [16, 17]. At 1 MeV, the mean free path is approximately 12.9 cm

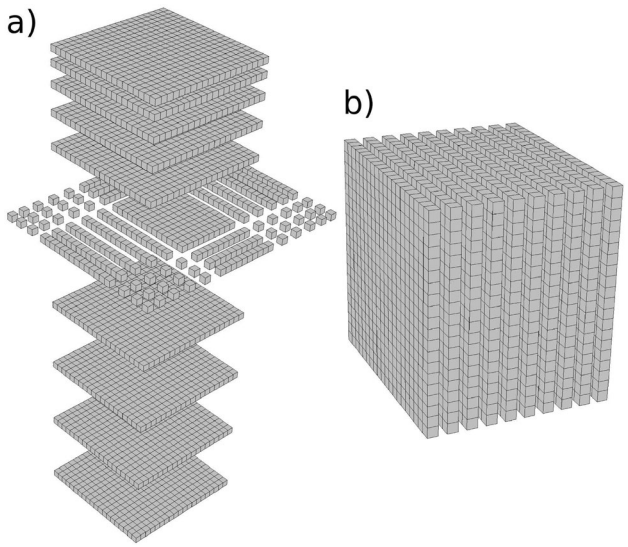

Fig. 2 **a** Exploded CAD drawing of how the scintillators of the proposed device may be distributed. This drawing serves to display the segmentation of the crystals and not the actual geometry of the detector. The cross-sectional face, the side facing the neutron source, is the side facing up. The cross section is 50 cm × 50 cm, and the depth is 25 cm. The top third of the drawing shows the compact layer arrangement that the detector would have and the bottom two thirds of the drawing are blown up to show the individual layers. The middle layer is further exploded to show the orientation of individual crystals. They are tightly arranged in each layer as shown in all other layers. **b** A more realistic view of the neutron detector with appropriate spacing. The cross-sectional face, the face closest to the source, is facing to the left of the page

spaced 20 mm apart. The detector is simulated in an idealized geometry where the crystals are packed tightly.

2.1 *p*-terphenyl

P-terphenyl [C_{18} H_{14}] is an organic crystalline scintillator. *P*-terphenyl has been of increased interest in fast-neutron detection during the past decade due to its large light output (about 20,000 ph/MeV [18]), excellent time resolution (477(12) ps [19]), fast decay time (14.1 ns [18]), and exceptional pulse shape discrimination (PSD), which gives us confidence for positive neutron identification with a good detection efficiency and fast response times. PSD is necessary to filter out γ-ray events from neutron events in the detector. γ rays from ambient background and from various reactions will swamp the detector, but with definitive PSD those events can be filtered out. Prior studies have shown that PSD in *p*-terphenyl is resolvable down to about the 100 keVee level [20, 21]. Current testing with a *pseudo-bar* configuration has shown accurate position resolution down to 300 keVee and PSD down to about 150 keVee [22]. In line with the previous studies, the PSD threshold used in the simulations was set to be at about the 100 keVee level.

3 MCNP6 simulations

Monte Carlo N Particle (MCNP6) [23] simulations were performed to estimate the performance of our detector. The simulations generated neutrons from an isotropic ^{235}U+n Watt fission source, which peaks at roughly 1 MeV in the neutron energy spectrum, and an ambient neutron background. Note that the ambient neutron background was produced by default functionality [24]. For the continental United States, there are 39 grid points where the ambient neutron background was sampled. Due to the proximity, the data point at ground level near New Orleans, Louisiana, was chosen. At this data point, the ambient neutron flux is 0.9907×10^{-2} n/cm^2/s. This results in approximately 100 neutrons/s entering our detector from background sources.

Our analysis of the neutron tracks included recoil energy calculations [25] and the PSD threshold explained in Sect. 2.1. All events below the PSD threshold were discarded.

4 Data analysis

4.1 Utilization of double- and single-scattering events

The location of the neutron source can be found using segmented neutron detector through observation of neutron double-scattering events (see, for example, Hamel et al. [14]). Application of this technique, in which a neutron needs to produce at least two signals in two separate crystals, in principle, is possible with the proposed detector system. The time of flight (TOF) for a fast neutron between two crystals may be small, but with the time resolution of around 600 ps for the *pseudo-bar* [22], most double-scattering events are resolvable. Figure 3 shows the simulated

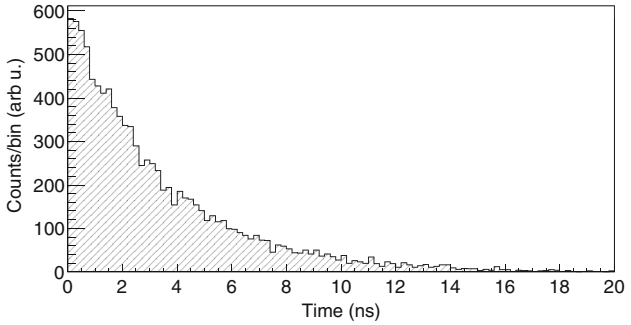

Fig. 3 The time of flight for a single neutron between two scattering events, where the scatterings happen in different crystals. The total neutrons simulated are arbitrary, and the ratio between different bins should be recognized

statistics of time difference between the first and second scattering events of the same neutron from the ^{235}U+n source. It is clear that significant fraction of double-scattering events can be resolved. While double-scattering technique offers an advantage of source localization, sole reliance on double-scattering events would reduce efficiency dramatically. Therefore, we will focus on single-scattering events in further discussion.

Our design of a highly segmented crystal array can utilize the density of scatterings in each of the crystals to detect the presence of the source. Crystals closest to the source will see more events than crystals further from the source due to the attenuation in the detector itself, and this effect is the key for identification of the localized source that increases neutron flux from one side of the detector.

4.2 Scattering distribution of directional neutrons and ambient neutron background

The proposed detector is specifically designed to be approximately two mean free paths for a 1-MeV neutron in *p*-terphenyl (Fig. 1). As shown in Fig. 4a, when we have a source located in front of the detector, we observe a large number of neutrons scattering in the first half. The number of source neutrons dramatically decreases with respect to the depth of the detector (Fig. 5). Figure 4b shows the relatively homogeneous distribution for hits from background neutrons. This background can be well characterized by periodic sampling of the background rate in each of the crystals.

5 Uniformly most powerful Bayesian tests

Uniformly most powerful Bayes tests (UMPBTs) [26] were used to define tests for positive identification. If a positive identification requires that the Bayes factor (i.e., likelihood ratio) for a test exceeds γ, then maximizing the

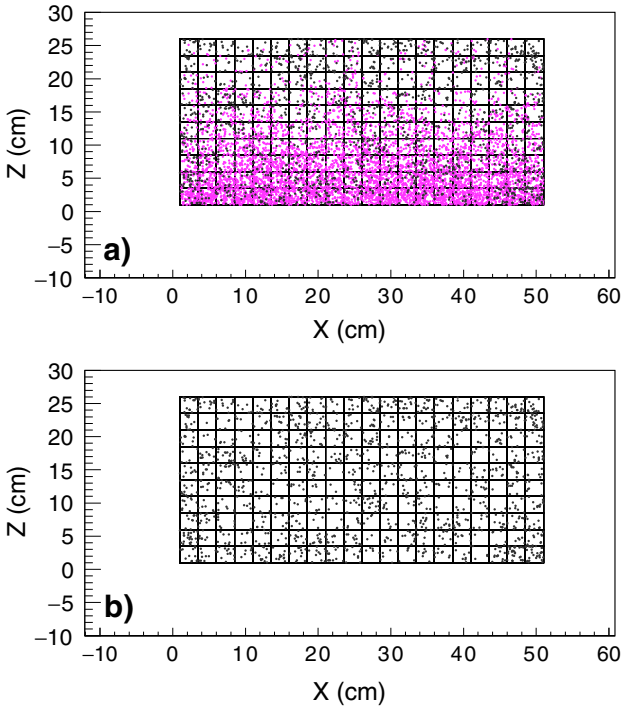

Fig. 4 (Color online) Scatterings of neutrons inside of the detector projected on the *x*-*z* plane. **a** Scattering neutrons are represented as dots due to both source neutrons (gray or magenta online) and ambient background neutrons (black). The ^{235}U+n neutron source is located in the middle of the detector on the *x* and *y* axes and at -100 cm on the *z*-axis. **b** The black dots are solely from ambient background neutrons

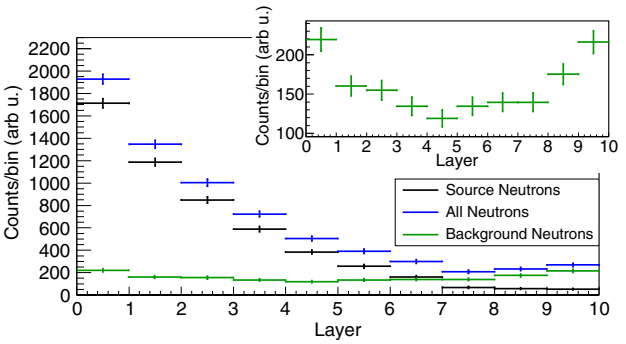

Fig. 5 Histogram showing the difference between source neutrons and background neutrons from Fig. 4a and comparing them to the total neutron count per layer of the detector. The source is positioned closest to layer 0 and furthest from layer 9. Layer zero refers to the bottommost row, and layer 9 refers to the topmost row in Fig. 4. The inset plot is a zoomed-in view of the background neutron counts with respect to the layer. The zoomed-in version clearly displays the relatively parabolic shape of the background, which is expected

probability of a positive identification can be accomplished by assuming the rate through the detector, λ_1 [n/s], which is chosen to maximize the function $f(\lambda_1)$, which corresponds to the number of counts in the detector, given by

$$f(\lambda_1) = \frac{\ln(\gamma) + \sum_j g(j)(\lambda_1 - \lambda_0)\Delta t}{\ln\left(\frac{\lambda_1}{\lambda_0}\right)}. \quad (1)$$

In this equation, background neutron rate is denoted by λ_0 and a total neutron rate is denoted by λ_1. A UMPBT threshold of γ is required to declare a positive identification; that is, $\gamma = 10^6$ means that the ratio of likelihoods evaluated at λ_1 and λ_0 is required to exceed 10^6 for detection. The function $g(j)$ is the average fraction of neutron scatterings per crystal j relative to the ambient neutron background simulated with MCNP6, and Δt is the real-world time that the simulation encompasses. For the purpose of the following calculations, $g(j)$ was averaged over 50 simulations of the ambient neutron background, with 10 million events each. The distribution of the number of counts in each crystal was fitted with Poisson function, providing the average, which was then normalized to the total ambient neutron flux. Naturally, the sum of all $g(j)$ is less than unity ($\Sigma g(j) = 0.244$) and specific values depend on the location of the crystal in the detector. In the real-life settings, these numbers can be directly measured periodically when there is no sample and corrected automatically (if necessary) in real time. The function $f(\lambda_1)$ is minimized with respect to λ_1 for a fixed time (Δt). This would give the minimum source intensity for which identification can be made at the required significance (γ) within a fixed time interval. Conversely, one can determine the minimum amount of time required to identify a source with a given intensity at the required level of significance.

The limit is set by:

$$\Sigma y_{ij} > f(\lambda_1), \quad (2)$$

where Σy_{ij} is the sum of events in the detector as a whole. The limit occurs when $\Sigma y_{ij} = f(\lambda_1)$, inferring that a source can be detected if it emits enough neutrons to satisfy Eq. (2).

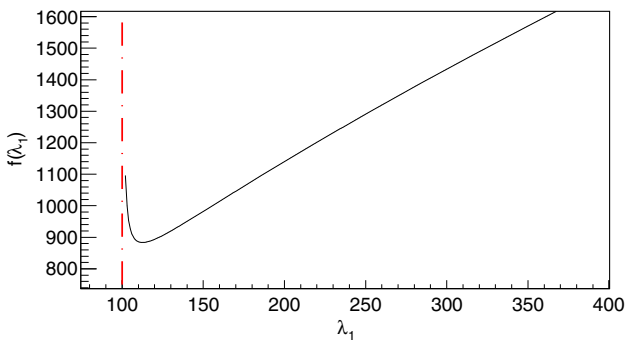

Fig. 6 Minimization of $f(\lambda_1)$ (Eq. (1)) with respect to λ_1, with Δt=32.13 seconds. The dashed line represents the location of λ_0. The trend of $f(\lambda_1)$ is asymptotic as it approaches λ_1=λ_0 and is approximately linear as it increases to infinity

The minimization of f(λ_1) is done by varying the value of λ_1. When f(λ_1) and λ_1 are plotted against one another, it is clear where the minimum lies (Fig. 6) for any given time interval of the measurements. The trend is asymptotic at $\lambda_1 = \lambda_0$, as expected.

By taking into account the geometric efficiency, the source neutron rate can be derived. The estimated number of source neutrons emitted per second is simply:

$$I_{\text{src,det}} = (\lambda_1 - \lambda_0), \quad (3)$$

$$I_{\text{src}} = I_{\text{src,det}} \times \frac{4\pi}{\Omega_{\text{sim}}}, \quad (4)$$

with $I_{\text{src,det}}$ being the number of neutrons emitted per second by the source within the solid angle covered by the detector active area. An intrinsic efficiency of the detector is given by:

$$\epsilon_{\text{sim}} = \frac{N_{\text{det,sim}}}{N_{\text{tot,sim}}} \times \frac{4\pi}{\Omega_{\text{sim}}}, \quad (5)$$

where $N_{\text{det,sim}}$ is the number of neutrons from the source that produce a signal above the threshold in the detector, $N_{\text{tot,sim}}$ is the total number of source neutrons in the simulation, and Ω_{sim} is the solid angle encompassed by the detector with respect to the point source in the simulation. The intrinsic efficiency is of course a function of energy threshold, which was set to a realistic value as explained in Sect. 3 in order to have clean neutron identification.

The time it takes for the detector to identify the source is then:

$$t = \frac{f(\lambda_1)/\epsilon_{\text{sim}}}{I_{\text{src}} \times \frac{\Omega}{4\pi}}, \quad (6)$$

where Ω is the solid angle from the source position being calculated.

As one may expect, the identification time scales with the solid angle and detector efficiency.

5.1 Comparison to industry standards

The National Committee on Radiation Instrumentation (NCRI) sets the requirements for radiation portal monitors. A Pacific Northwest National Laboratory (PNNL) study (Kouzes et al.) in 2010 describes the requirements for alternative neutron portal monitors for the current ^{3}He monitors [27]. Following the parameters discussed in this study, the fulfillment of requirements is tested. The requirements set is in terms of ^{252}Cf spontaneous fission, which has a notable conversion of 1 ng to 2.1×10^3 n/s. The efficiency requirement for an alternative neutron monitor is 2.5 cps/ng (counts per second per nanogram) for a source 2 m away from the detector. The source is also

required to be moderated by 2.5 cm of polyethylene. The ^{252}Cf source used emitted a total of 950,000 neutrons over a span of 1.388 seconds. This source intensity corresponds to a source of 326 ng.

The ^{252}Cf source and a 2.5-cm-thick polyethylene wall were implemented in an MCNP6 simulation to reconstruct the tests of the ^{3}He detector from Kouzes et al. [27]. The specific geometry was duplicated according to previous MCNP simulations for the detector [1]. A single ^{3}He tube at 3 atm was used for this simulation. The simulations yielded a neutron rate of 597 n/s being detected, which corresponds to an efficiency of 1.83 cps/ng. The difference between this efficiency and the quoted 3.0 cps/ng is likely due to the undefined polyethylene thickness of the real ^{3}He detector.

A comparative simulation was constructed with the proposed detector replacing the ^{3}He detector. The simulation yielded a neutron rate of 3203.22 n/s after a 2.5-cm-thick polyethylene moderator. It should be noted, however, that the polyethylene moderator is not necessary for the proposed detector apparatus, but included in order to comply with the NCRI standards and make a direct comparison to previous studies. This rate corresponds to an efficiency of 9.83 cps/ng. The efficiency then needed to be normalized to the size of the ^{3}He detector. Normalization was done based on the ratio of the volumes of the two detectors, which provides only an estimate for the scaling of the efficiency. The total volume of the ^{3}He detector is 170,190 cm^3 (183 cm $\times$ 15 cm $\times$ 62 cm) [1], and the total volume of the proposed detector is 62,500 cm^3. This leads to a detection efficiency of 26.8 cps/ng that is directly comparable to the previous study. Table 1 shows the comparison of the calculated efficiency of the proposed detector to commercially available detectors tested in Kouzes et al. [27].

In order to make a direct comparison to the ^{3}He detector, positive detection confidence levels were calculated for a ^{252}Cf source (rate of 3112 n/s) at a distance of 2 m from the detector and at various exposure times. A series of 50 MCNP simulations were performed for each time with and without a source present. A Poisson average was taken for the sets of 50 simulations to get the average number of neutrons detected from the source, C_{src}, and from the background, C_{BG}. For each exposure time, the error on the background was calculated as:

$$\epsilon = \sqrt{C_{\mathrm{BG}}}. \tag{7}$$

With ϵ, the confidence interval was calculated with:

$$x = \frac{C_{\mathrm{Total}} - C_{\mathrm{BG}}}{\epsilon}, \tag{8}$$

with C_{Total} being the sum of C_{src} and C_{BG}. The confidence interval was then used to calculate the confidence level in the form 1 in γ, with:

Table 1 Comparison of neutron detection efficiency of the proposed detector and commercially available detectors studied in Kouzes et al. [27]

Detector type	Efficiency (cps/ng)
Proposed Detector - Without UMPBT	26.8
^{3}He proportional detector (1 tube)	3.0(2)†
BF_3 proportional detector (3 tubes)	3.7(2)†
Boron-lined proportional detector	3.0(2)†
Lithium-loaded glass fibers	1.7(6)†
Coated non-scintillating plastic fibers	2.0(1)†

Values marked with a † were taken from Kouzes et al.

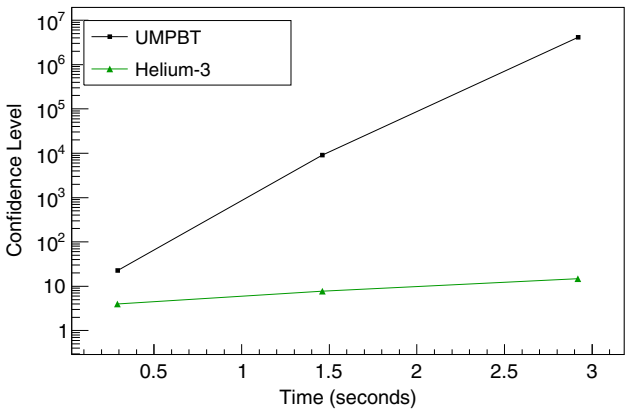

Fig. 7 Confidence levels γ (i.e., γ=10^6 corresponds to a confidence level of 1 in 10^6) calculated for a ^{3}He detector (triangles and green online) and the proposed detector (squares and black) using the UMPBT model. The confidence levels were derived from sets of 50 MCNP simulations with and without a source present. The confidence levels show a sensitivity comparison of the proposed detector to a standard ^{3}He detector

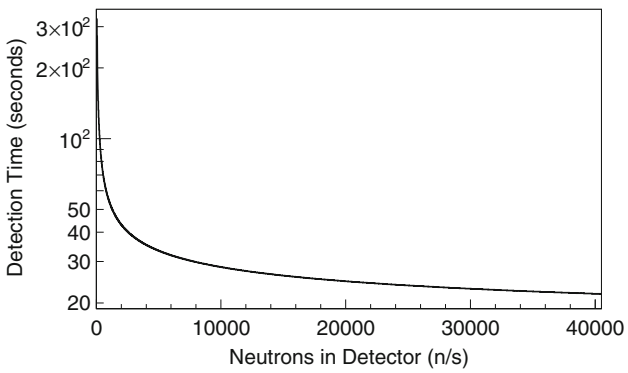

Fig. 8 Detection time vs source-neutron intensity entering the detector. The plot is in logarithmic scale. The confidence level used is γ=10^6

Table 2 ^{235}U+n neutron source intensity vs time needed to identify the source at various distances

Source distance (m)	$I_{src,det}$ (n/s)	I_{src} (n/s)	Time (sec)
1	1	50.3	16,703
	10	502.7	1477
	100	5027	192
	200	10,053	120
	800	40,212	60
2	50	10,053	331
	200	40,212	120
3	22	9953	686
	89	40,263	209
5	8	10,053	1851
	32	40,212	487
10	2	10,053	7966
	8	40,212	1851

The source is centered on the face of the detector, and the distance is the distance of the source relative to the detector. The time was found using the UMPBT statistical model and represents the minimum time, with the assumptions previously stated, that it would take to positively identify a neutron source. The confidence level used is γ=10^6

Table 3 Source-neutron intensity entering the detector, with a source distance of one meter, and the mass conversion for ^{235}U

$I_{src,det}$ $\times 10^3$ (n/s)	Mass (g)	Time (sec)
0.01	0.0081	1477
0.1	0.0807	192
0.2	0.161	120
0.8	0.646	59.8
1.5	1.21	47.4
2	1.61	43.1
3	2.42	38.2
4	3.23	35.3
5	4.03	33.4
10	8.07	28.4
25	20.2	23.7

The detection times found for the various masses at one meter from the detector are also displayed. The confidence level used is γ=10^6

$$\gamma = \frac{1}{1 - Erf\left(\frac{x}{\sqrt{2}}\right)}. \tag{9}$$

Similarly, the confidence level for the UMPBT model was found using the same data with Eq. (1). Figure 7 shows the abundant sensitivity advantage that the proposed detector (with the UMPBT model) has over a ^{3}He detector.

5.2 Active interrogation technique with the proposed detector

Since the proposed detector uses fast neutrons to detect the presence of fissile material, it becomes possible to use a beam of low-energy neutrons for active interrogation. It is one of the key advantages of the proposed detector system. In particular, it is shown in Ref. [9] that 60 keV neutrons produced by ^{7}Li(p,n)^{7}Be neutron generator can be utilized for this purpose. For the case of ^{235}U, the UMPBT model can be used to estimate the minimum time required to detect a fissile material under active interrogation. Plotting the two calculated values (Eqs. (3) and (6)) against one another provides a sensitivity limitation trend for our detector (Fig. 8). Table 2 shows the minimum time it would take to detect various source strengths at various distances.

The source intensity was converted into mass to determine how much of the material must be present in order to be detectable. We assume that neutron flux for a 60 keV beam is $\phi = 5 \times 10^6$ cm $^{-2}$ s^{-1}, as in Ref. [9]. The fission cross section, $\sigma \approx 2$ barns [28] at 60 keV, and the prompt neutron multiplicity, $\nu_p = 2.42$ [28], of the ^{235}U+n reaction were used. Using equation (10), Avagadro's number, N_A, and the mass $M_{^{235}U} = 235$ g, the conversion was performed to estimate the mass for a range of source neutron intensities (Table 3). A similar plot to Fig. 8 was then made with respect to mass (Fig. 9).

$$M = \frac{I_{src}}{\nu_p N_A \sigma \phi} M_{^{235}U} \tag{10}$$

It is clear that the proposed detector system becomes extremely sensitive to even very small amounts of fissile material under active interrogation. Figures 8 and 9 indicate that 1 g of ^{235}U can be detected in less than a minute if

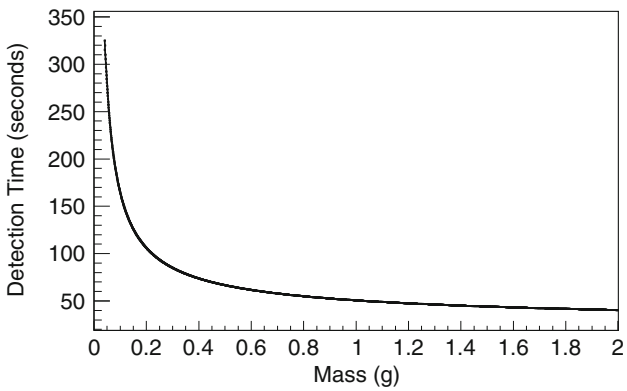

Fig. 9 Similar to Fig. 8, but in terms of mass of ^{235}U instead of source-neutron intensity. The confidence level used is γ=10^6

modest flux of 5×10^6 cm^{-2} s^{-1} of 60 keV neutrons is used for active interrogation. Note that it is not possible to use systems based on thermal neutron detection in this case because of the background which will be unavoidably caused by the interrogating neutron beam.

6 Summary and conclusion

Special nuclear materials should be carefully monitored and controlled. The monitoring of these materials is of critical importance for global security, especially weapons-grade plutonium and highly enriched uranium. Detection of these materials can be facilitated by active interrogation with low-energy (<100 keV) neutrons. Even without active interrogation, our proposed detector design and analysis method overcomes the limitations set by thermal-neutron detectors as well as the higher false alarm rate of γ-ray detectors.

Using MCNP6 simulations and the uniformly most powerful Bayesian tests statistical model, the limits of the proposed detector were probed. For a fissile material undergoing fission one meter away from the detector, without any moderation, it would take about 25 min to identify a source emitting ≈500 n/s, and similarly 192 seconds for ≈5000 n/s. For the specific case for ^{235}U+n, with the specific parameters discussed in Sect. 5.2, these limits translate to 8.1 mg and 80.7 mg of ^{235}U, respectively.

Comparisons to commercially available neutron detectors, studied in Kouzes et al. [27], were made (Table 1). The requirements set by the National Committee on Radiation Instrumentation at the time of the previous study required a minimum neutron detection efficiency of 2.5 cps/ng. The detector proposed in the current work surpasses that requirements set. The proposed detector performs with an efficiency of 26.8 cps/ng. With the UMPBT model, a comparison of confidence levels for a particular source at various exposure times revealed a significant increase in sensitivity compared to the ^{3}He detector (Fig. 7). With respect to the previously studied detectors described in Kouzes *et al.*, the proposed neutron detection has a significant advantage in efficiency and sensitivity.

Our method can be applied to the development of a monitoring device and the times produced scale linearly with the solid angle of the detector with respect to the source. Increasing the number of the proposed detectors in various positions around the source will increase the sensitivity and reduce the required detection time of the detector significantly.

Authors' contributions All authors contributed to the design of the detector and the methodology of the study. Simulations and analyses were performed by Eric Aboud with assistance by Sunghoon Ahn. The UMPBT model was provided by Valen E. Johnson. The first draft of their manuscript was written by Eric Aboud, and all authors provided feedback on drafts of the manuscript. All authors read and approved the final manuscript.

References

1. R.T. Kouzes, E.R. Siciliano, J.H. Ely et al., Passive neutron detection for interdiction of nuclear material at borders. Nucl. Instrum. Methods A **584**, 383–400 (2008). https://doi.org/10.1016/j.nima.2007.10.026
2. J.L. Lacy, A. Anthanasiades, C.S. Martin et al., Straw-based portal monitor ^{3}He replacement detector with expanded capabilities. IEEE Nucl. Sci. Conf. R 4865–4868 (2011). https://doi.org/10.1109/NSSMIC.2011.6152486
3. R.T. Kouzes, J.H. Ely, PNNL-19360: status summary of ^{3}He and neutron detection alternatives for homeland security (2010)
4. D.A. Shea, L. Daniel, *The Helium-3 Shortage: Supply, Demand, and Options for Congress* (Congressional Research Service, Washington, DC, 2010)
5. P.E. Vanier, L. Forman, R. Daren, Thermal neutron imaging in an active interrogation environment. AIP Conf. Proc. **1099**, 583 (2009). https://doi.org/10.1063/1.3120104
6. C.E. Moss, C.L. Hollas, G.W. McKinnety et al., Comparison of active interrogation techniques. IEEE Nucl. Sci. Conf. R **2005**, 329–332 (2005). https://doi.org/10.1109/NSSMIC.2005.1596264
7. R.C. Runkle, D.L. Chichester, S.L. Thompson, Rattling nucleons: new developments in active interrogation of special nuclear material. Nucl. Instrum. Methods A **663**, 75–95 (2011). https://doi.org/10.1016/j.nima.2011.09.052
8. D. Dietrich, C. Hagmann, P. Kerr et al., A kinematically beamed, low energy pulsed neutron source for active interrogation. Nucl. Instrum. Meth. B **241**, 826–830 (2005). https://doi.org/10.1016/j.nimb.2005.07.139
9. C.A. Hagmann, D.D. Dietrich, J.M. Hall et al., Active detection of shielded SNM with 60-keV neutrons. IEEE Trans. Nucl. Sci. **56**, 1215–1217 (2009). https://doi.org/10.1109/TNS.2009.2012859
10. P. Kerr, M. Rowland, D. Dietrich et al., Active detection of small quantities of shielded highly-enriched uranium using low-dose 60-kev neutron interrogation. Nucl. Instrum. Methods B **261**, 347–350 (2007). https://doi.org/10.1016/j.nimb.2007.04.190
11. P.B. Rose, A.S. Erickson, M. Mayer et al., Uncovering special nuclear materials by low-energy nuclear reaction imaging. Sci. Rep. **6**, 24388 (2016). https://doi.org/10.1038/srep24388
12. M.C. Hamel, J.K. Polack, M.L. Ruch et al., Active neutron and gamma-ray imaging of highly enriched uranium for treaty verification OPEN. Sci. Rep. **7**, 7997 (2017). https://doi.org/10.1038/s41598-017-08253-x
13. P. Hausladen, M. Blackston, E. Brubaker et al., Fast neutron coded-aperture imaging of special nuclear material configurations. 53rd Annual Meeting of the INMM (2012)
14. M.C. Hamel, J.K. Polack, A. Poitrasson-Rivière et al., Stochastic image reconstruction for a dual-particle imaging system. Nucl. Instrum. Methods A **810**, 120–131 (2016). https://doi.org/10.1016/j.nima.2015.12.002
15. C. Meegan, G. Lichti, P.N. Bhat et al., The Fermi gamma-ray burst monitor. Astrophy. J. **702**, 791–804 (2009). https://doi.org/10.1088/0004-637X/702/1/791
16. D.A. Brown, M.B. Chadwick, R. Capote et al., ENDF/B-VIII.0: the 8th major release of the nuclear reaction data library with

CIELO-project cross sections, new standards and thermal scattering data. Nucl. Data Sheets **148**, 1–142 (2018). https://doi.org/10.1016/j.nds.2018.02.001
17. M.B. Chadwick, M. Herman, P. Obložinský et al., ENDF/B-VII.1 nuclear data for science and technology: cross sections, covariances, fission product yields and decay data. Nucl. Data Sheets **112**, 2887–2996 (2011). https://doi.org/10.1016/j.nds.2011.11.002
18. T. Yanagida, K. Watanabe, Y. Fujimoto, Comparative study of neutron and gamma-ray pulse shape discrimination of anthracene, stilbene, and p-terphenyl. Nucl. Instrum. Methods A **784**, 111–114 (2015). https://doi.org/10.1016/j.nima.2014.12.031
19. A. Sardet, C. Varignon, B. Laurent et al., p-Terphenyl: an alternative to liquid scintillators for neutron detection. Nucl. Instrum. Methods A **792**, 74–80 (2015). https://doi.org/10.1016/j.nima.2015.04.038
20. J. Iwanowska, L. Swiderski, M. Moszynski et al., Neutron/gamma discrimination properties of composite scintillation detectors. J. Instrum. **6**, P07007 (2011). https://doi.org/10.1088/1748-0221/6/07/P07007
21. M.L. Ruch, M. Flaska, S.A. Pozzi, Pulse shape discrimination performance of stilbene coupled to low-noise silicon photomultipliers. Nucl. Instrum. Methods A **793**, 1–5 (2015). https://doi.org/10.1016/j.nima.2015.04.053
22. D.P. Scriven, G. Christian, G.V. Rogachev et al., A position and pulse shape discriminant p-terphenyl detector module. Nucl. Instrum. Methods A **1010**, 165492 (2021). https://doi.org/10.1016/j.nima.2021.165492
23. T. Goorley, M. James, T. Booth et al., Initial MCNP6 release overview. Nucl. Technol. **180**, 298–315 (2012). https://doi.org/10.13182/NT11-135
24. G.E. McMath, G.W. McKinney, T. Wilcox, MCNP6 Cosmic & Terrestrial Background Particle Fluxes–Release 4 (2015)
25. C. Matei, F.J. Hambsch, S. Oberstedt, Proton light output function and neutron efficiency of a p-terphenyl detector using a 252Cf source. Nucl. Instrum. Methods A **676**, 135–139 (2012). https://doi.org/10.1016/j.nima.2011.11.076
26. V.E. Johnson, Uniformly most powerful Bayesian tests. Ann. Stat. **41**, 1716–1741 (2013). https://doi.org/10.1214/13-AOS1123
27. R.T. Kouzes, J.H. Ely, L.E. Erikson et al., Alternative neutron detection testing summary. PNNL (2010)
28. K. Shibata, O. Iwamoto, T. Nakagawa et al., JENDL-4.0: a new library for nuclear science and engineering. J. Nucl. Sci. Technol. **48**, 1–30 (2011). https://doi.org/10.1080/18811248.2011.9711675